Geochemistry, Geophysics, Geosystems

RESEARCH ARTICLE
10.1029/2018GC008067

Key Points:
- Decrease of sedimentation rate is in Lake Yamanaka observed following scoria fallout
- Lake Yamanaka's sedimentary system took over ~170 years to recover its initial sedimentation rate
- Anthropogenic modifications of the catchment have a greater impact than a major Plinian eruption of Mount Fuji on the sedimentation rate

Supporting Information:
- Supporting Information S1
- Table S1
- Table S2
- Table S3
- Table S4
- Figure S1

Correspondence to:
L. Lamair,
laura.lamair@uliege.be

Citation:
Lamair, L., Hubert-Ferrari, A., El Ouahabi, M., Yamamoto, S., Schmidt, S., Vander Auwera, J., et al. (2019). Late Holocene changes in erosion patterns in a lacustrine environment: Landscape stabilization by volcanic activity versus human activity. *Geochemistry, Geophysics, Geosystems*, *20*. https://doi.org/10.1029/2018GC008067

Received 16 NOV 2018
Accepted 7 FEB 2019
Accepted article online 8 MAR 2019

Late Holocene Changes in Erosion Patterns in a Lacustrine Environment: Landscape Stabilization by Volcanic Activity Versus Human Activity

Laura Lamair[1,2], Aurélia Hubert-Ferrari[1], Meriam El Ouahabi[3], Shinya Yamamoto[4], Sabine Schmidt[5], Jacqueline Vander Auwera[3], Gilles Lepoint[6], Evelien Boes[7], Osamu Fujiwara[8], Yusuke Yokoyama[9], Marc De Batist[7], and Vanessa M. A. Heyvaert[2,7]

[1]Department of Geography, University of Liège, Liège, Belgium, [2]Geological Survey of Belgium, Royal Belgian Institute of Natural Sciences, Brussels, Belgium, [3]Department of Geology, University of Liège, Liège, Belgium, [4]Mount Fuji Research Institute, Yamanashi Prefectural Government, Yamanashi, Japan, [5]UMR5805 EPOC, CNRS, University of Bordeaux, Pessac, France, [6]Laboratory of Oceanology, University of Liege, Liège, Belgium, [7]Department of Geology, Ghent University, Ghent, Belgium, [8]Geological Survey of Japan, National Institute of Advanced Industrial Science and Technology, Tsukuba, Japan, [9]Atmosphere and Ocean Research Institute, University of Tokyo, Chiba, Japan

Abstract The most recent eruption of Mount Fuji (Japan), the VEI 5 Hōei plinian eruption (CE 1707) heavily impacted Lake Yamanaka, a shallow lake located at the foot of Mount Fuji. Here we discuss the influence of the Hōei eruption on the lacustrine sedimentation of Lake Yamanaka using high-resolution geophysical and geochemical measurements on gravity cores. Hōei scoria fallout had two major impacts on Lake Yamanaka: (i) reduction of the sedimentation rate (from ~0.16 to ~0.09 cm/year) and (ii) the increase of in situ lake productivity. Sedimentation rates after the eruption were relatively low due to the thick scoria layer, trapping underlying sediments in the catchment. The lacustrine system took more than ~170 years to begin to recover from the Hōei eruption: most recently sedimentation recovery has been accelerated by changes in land use. Since the beginning of the twentieth century, vegetated strips delimited cultivated parcels, trapping sediment and minimizing anthropogenic impacts on the sedimentation rate. Over the last decade, the decline of agriculture and the increase of other human activities has led to an increase in the sedimentation rate (~1 cm/year). This study highlights the effect of the grainsize of the volcanic ejecta on the sedimentation rate following a volcanic eruption. Coarse-grained tephra are difficult to erode. Therefore, their erosion and remobilization is largely limited to intense typhoons when porous scoria deposits are saturated by heavy rains. Moreover, this study suggests that recent anthropogenic modifications of the catchment had a greater impact on the sedimentation rate than the Hōei eruption.

1. Introduction

Large explosive Plinian eruptions are known to cause landscape changes and sedimentological processes over extended areas. Intense erosion and deposition occurs following major eruptions (e.g., Collins et al., 1983; Collins & Dunne, 1986; Hayes et al., 2002). Large volumes of unconsolidated ash fall deposits are easily remobilized by fluvial and mass-flow processes, the vegetation cover is destroyed and drainage networks are modified following an eruption (e.g., Hayes et al., 2002; Major et al., 1996, 2016; Ollier & Brown, 1971; Pierson et al., 1992, 2013; Pierson & Major, 2014). Landscape recovery and its duration depend on different controlling factors such as the preeruption geomorphology, the volume, type, and distribution of erupted materials and the local climatic conditions (Manville, Nemeth, et al., 2009; Manville, Segschneider, et al., 2009; Manville & Wilson, 2004). Erosion is influenced by the thickness and the grain size of the tephra deposit (Folsom, 1986). Following an eruption, thick and coarse-grained tephra deposits are difficult to erode due to their high permeability and resistance to rain splash erosion. White et al. (1997) show that deposits of the CE 1886 Mount Tarawera eruption (New Zealand) remained in place until 18 years later, when breakout flood from volcanically dammed Lake Tarawera initiated large-scale erosion and redeposition. The latter suggest that high energy events are required to induce the erosion of coarse well sorted and highly permeable tephra deposits. The above-mentioned studies discuss the role fluvial and mass transport processes play in posteruption landscape recovery. However, at present, the short-term and long-term impact of coarse

scoria fall deposits on lacustrine sedimentation processes and lake recovery is unknown. Here we document the first example of an explosive volcanic eruption that increased landscape stability and reduced erosion and sedimentation rates.

We study Lake Yamanaka, part of the Fuji Five Lakes region (Japan), an area that is both affected by large Plinian eruptions from Mount Fuji and high energy events (typhoons and earthquakes). Due to the westerly wind direction and its proximity to the volcano, Lake Yamanaka and its catchment have been repeatedly strongly impacted by scoria fallout. The last eruption of Mount Fuji, called the Hōei eruption, occurred in CE 1707 and lasted 16 days from the 16 December 1707 until the 1 January 1708 (Tsuya, 1955). In total, 1.8 km^3 of scoria fallout were ejected from three vents located in the southeastern flank of the volcano (Figure 1; Miyaji et al., 2011). The thickness of the scoria deposit varies from 5 to 37 cm around Lake Yamanaka and reaches up to 64 cm (on average) at the southwest extremity of its catchment (Miyaji et al., 2011). Lake Yamanaka and its catchment have also been affected by an increase in human occupation and activities over the last century. The primary objectives of this study are: (1) to study the influence of a Plinian eruption (i.e., Hōei eruption) on the sedimentation of Lake Yamanaka; (2) to assess the process of sedimentation recovery following a major eruption; (3) to evaluate recent anthropic effects on the lacustrine sedimentation of Lake Yamanaka. We present a detailed study of the sedimentation history of Lake Yamanaka since the Hōei eruption (CE 1707).

2. Study Area

Lake Yamanaka (35.4185°N, 138.8787°E at the center of the lake; 981 m above sea leavel; Figure 1) has a maximum depth of 14.3 m and is located at the foot of the East-North-East flank of Mount Fuji (3,776 m above sea level). Lake Yamanaka covers a surface area of 6.89 km^2 and is fed by underground water originating from the Mount Fuji and Tanzawa mountains aquifers via springs located at its bottom (Hirabayashi et al., 2004; Koshimizu & Tomura, 2000). The lake receives additional water inputs by ephemeral rivers, active during typhoons, spring time (snow melting), and torrential rain episodes. The Katsura River, located at the northwestern end of Lake Yamanaka, is fed by the lake and flows into Sagami Bay (Pacific Ocean).

The catchment of Lake Yamanaka has an asymmetric shape with an area of 69.81 km^2. The East-North-East flank of Mount Fuji constitutes 51% of the catchment and is characterized by gentle slopes (~2–5°). Toward the north, the watershed is limited and has steep slopes (~13–18°). The catchment is mainly composed of basalt lava flows, lahar, and pyroclastic fall deposits.

3. Materials and Methods

3.1. Sediment Cores

The core data set is composed of five short gravity cores (YAM14-1A, YAM14-2A, YAM14-3B, YAM14-4B, and YAM14-5B) collected using a gravity Uwitec corer system during October 2014 (Figure 1). The length of the cores ranges between 39.9 and 66.5 cm: all the cores terminated in the top of a coarse scoria layer. The cores were split, described, and scanned for imagery (linescan) and physical properties using a Geotek MSCL core scanner. Core-to-core correlations were done based on magnetic susceptibility (Figure 2). X-ray radiography was performed on all the cores to identify sedimentary structures not visible to the naked eye.

We selected core YAM14-2A, located in the deepest part of the lake, to perform high-resolution measurements. This core is inferred to be representative of the background sedimentation (i.e., hemipelagite). Due to its distal location from sedimentary sources, it only records major sedimentary disturbances. Grain size analysis was performed using a Malvern 2000 at a 0.5-cm sampling interval. To avoid clay flocculation, 2 ml of 0.5-g/L sodium hexametaphosphate was added. Scanning electron microscopy and smear slides were carried out on selected samples to characterize the background sedimentation. Semiquantitative elemental composition was done using an Avaatech X-ray fluorescence (XRF) core scanner at a resolution of 2 mm and under two different conditions (for light elements: 0.1 mA, 10-s count time, and 10 kV; for heavier ones: 0.75 mA, 45-s count time, and 30 kV). Only significant chemical elements (more than 1,000 counts per second) are considered. Data were not smoothed allowing the detection of minor shifts along the core. Reliable data were obtained for Al, Si, S, Ca, Ti, Mn, Fe, Cu, Zn, Br, Sr, Zr, and Pb. The Si/Zr

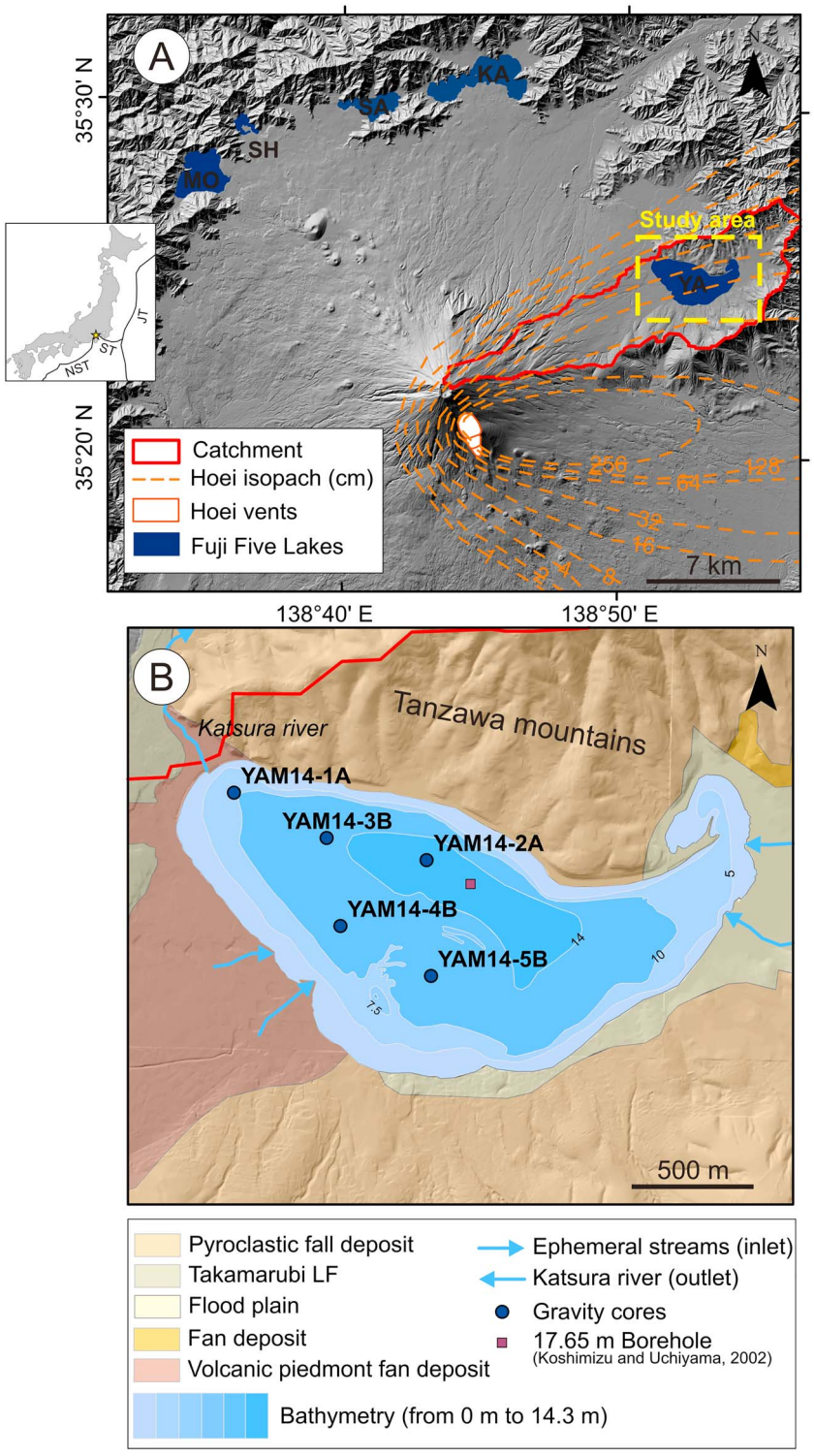

Figure 1. General settings. (a) Location map of Lake Yamanaka (YA) and Fuji Five Lakes region (MO = Lake Motosu, SH = Lake Shoji, SA = Lake Sai, and KA = Lake Kawaguchi). Isopachs represent the direction and the thickness of the tephra fallout produced by the Hoei eruption (CE 1707; after Miyaji et al., 2011). (b) Study area showing geological map (Ozaki et al., 2002) and bathymetric map of Lake Yamanaka (Adhikari et al., 2005). Lake Yamanaka is very shallow with a maximum depth of 14.3 m. Inlets and outlets of Lake Yamanaka are represented with the blue arrow. Its catchment mainly consists of volcaniclastic and pyroclastic deposits.

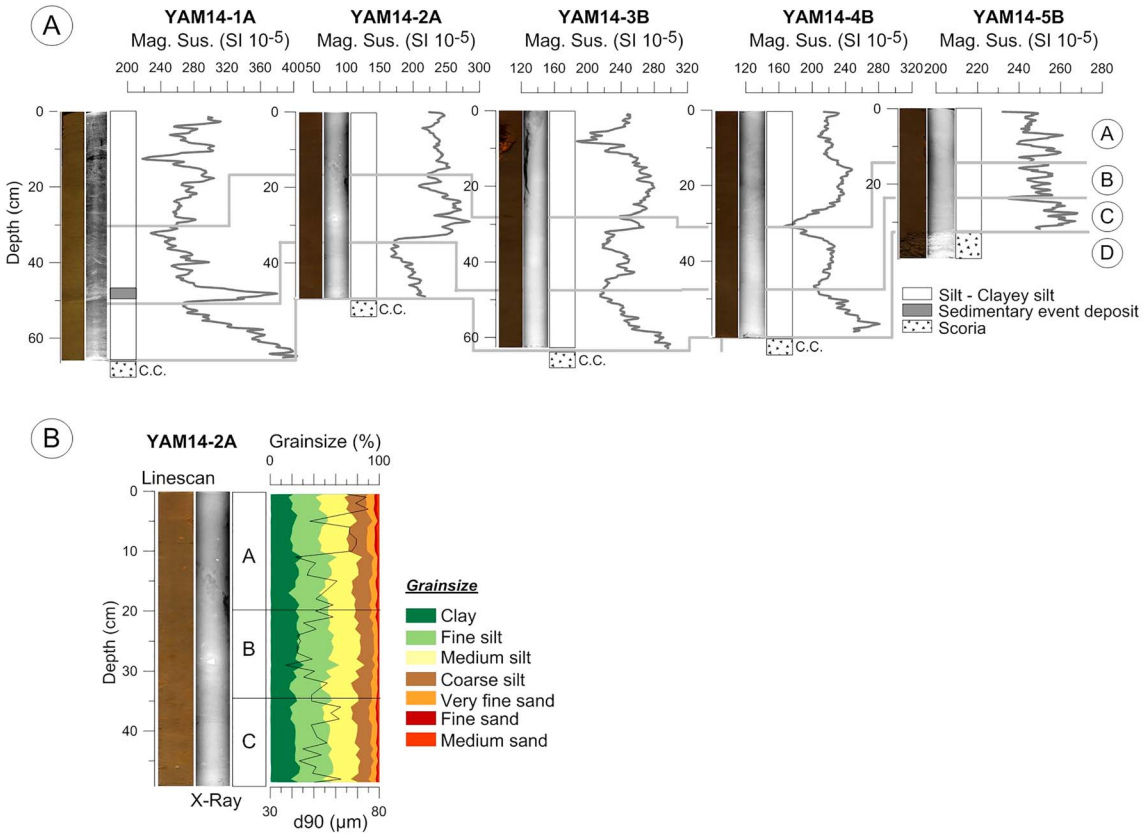

Figure 2. Core to core correlations based on magnetic susceptibility (Mag. Sus.). (a, left to right) Linescan, X-ray photography, schematic log, and magnetic susceptibility depth profile. The sedimentary record are divided into four sedimentary units (A to D). D corresponds to the Hōei scoria deposits and is recorded at the base of YAM14-5A and in all the core catchers (C.C.). (b) Grain size analysis done on YAM14-2A.

ratio was employed to estimate the biogenic silica content relative to material (Cuven et al., 2011) and Br/Ti as a proxy for organic productivity (e.g., Agnihotri et al., 2008). We built a correlation matrix for each sedimentary unit to assess the quality of the correlation between pairs of elements (Kylander et al., 2011; see supporting information S1). R values greater than 0.7 or lower than −0.7 were considered as strong correlations. The disadvantage of the Avaatech core scanner is that Al is the lightest element, which can be measured under reasonable exposure times, and elements present at low concentrations are poorly constrained. In order to validate the elemental variations measured by the Avaatech core scanner, major (Si, Ti, Al, Fe, Mn, Mg, Ca, Na, and K) and trace elements above 500 ppm (Ba, Cr, Cu, Ni, Sr, P, Zr, Zn, Co, and Pb) were measured in 10 selected samples using XRF spectrometry (PERFORM′X) on pressed powdered pellets.

XRD spectra were acquired at 1-cm resolution using a PANalytical Empyrean XRD and were processed with DIFFRAC.EVA software. Clay analysis was performed on selected samples. For that purpose, the clay fraction (<2 µm) was separated by settling in a water column and mounted as oriented aggregates on glass slides (Moore & Reynolds, 1989). Three X-ray spectra were acquired on slides prepared under different experimental conditions: (i) air-dried, (ii) ethylene glycol solvated for 24 hr, and (iii) heated at 500 °C for 4 hr.

$\delta^{13}C$, $\delta^{15}N$, TOC (total organic carbon), and TN (total nitrogen) analyses were performed on bulk sediments at 1-cm resolution. C/N values were derived from the TOC and the TN data. The C/N atomic ratio provides information about the origin of the organic matter (OM). Terrestrial plants are characterized by a C/N value around 20 or greater, whereas lacustrine phytoplankton show low C/N ratio, between 3 and 9. A mixed source generally has C/N value ranging from 10 to 20 (e.g., Meyers, 1994). Every centimeter of the core was sampled for loss on ignition. The samples were dried at 105 °C for 24 hr and then heated at 550 °C for 24 hr. The water and OM content were calculated following Heiri et al. (2001).

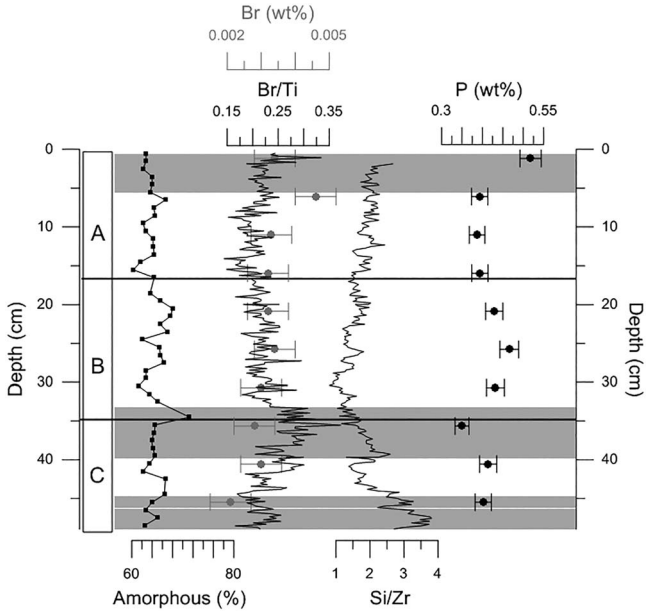

Figure 3. Depth profiles of the elements selected for study measured on YAM14-2A. (left to right) Percentage of amorphous materials, Br/Ti ratio, Br (%wt), Si/Zr ratio, and P (wt%). On the P (wt%) depth profile, error bars correspond to the instrumental error. Sedimentary boundaries (A–C) defined based on the magnetic susceptibility are also indicated. The peaks mentioned in the main text are highlighted in gray. Peaks of Si/Zr are interpreted as increase of diatoms content. The upper 5 cm of the gravity core present enrichment in P related to recent eutrophication.

3.2. Chemostratigraphy

Four sedimentary units (from A to D) were defined based on lithology, magnetic susceptibility, XRF, and isotopic measurements. The oldest sedimentary unit, unit D, corresponds to a black scoria layer deposited during the last eruption of Mount Fuji, the CE 1707 Hōei eruption. Its identification was done based on its stratigraphic position and on the isopach map of the Hōei tephra fallout (Figure 1a). The absence of OM and silt intercalated within the scoria deposits suggest that the scoria has not been reworked. The primary deposit nature is also supported by high-resolution seismic reflection profiling where the Hōei scoria deposits appear as undisturbed and continuous strong reflective horizons (Lamair et al., 2019). The boundary between unit D and unit C is defined by a change in lithology (from scoria to lacustrine sediments). The boundary between unit C and unit B is marked by a significant minimum in the magnetic susceptibility depth profile. The boundary between unit B and unit A corresponds to an increase of $\delta^{15}N$. This boundary is supported by a change of slope in $^{210}Pb_{xs}$ depth profile (see the following section).

3.3. Age-Depth Model

Short lived radionuclides (^{210}Pb, ^{226}Ra, and ^{137}Cs) were used to define the chronology of the sedimentary infill of Lake Yamanaka over the last century by sampling selected 1-cm-thick layers in the upper 32 cm of core YAM14-2A. Activities of ^{210}Pb, ^{226}Ra, and ^{137}Cs were measured by gamma spectrometry using a high-efficiency, well-type detector (Ge volume 280 cm^3, CANBERRA; Schmidt & De Deckker, 2015). Activities are expressed in millibecquerels per gram, and errors are based on one standard deviation counting statistics. Excess ^{210}Pb ($^{210}Pb_{xs}$) was calculated by subtracting the activity supported by its parent isotope, ^{226}Ra, from the total ^{210}Pb activity in the sediment.

In order to estimate the sedimentation rate and the age of the lacustrine sediments, two models were applied: the constant flux constant sedimentation (CF/CS) model (Oldfield & Appleby, 1984) and the constant initial concentration model. In addition to ^{210}Pb and ^{137}Cs dating, the CE 1707 Hōei scoria layer was used as a temporal marker. The age of the upper boundary of Unit C was deduced from the sedimentation rate obtained for Unit B.

4. Results

4.1. Description of the Sedimentary Deposits

The sedimentary sequence recovered in the cores consists of homogenous gray brown silt. A thick black basal scoria layer of 6.4 cm is recorded in core YAM14-5A as well as in all core catchers (Figure 2). No cores penetrate to the base of this scoria layer. Based on its stratigraphic position, the scoria deposit is associated with the last eruption of Mount Fuji, the Hōei eruption (CE 1707). The water content of the short cores ranges from 76% to 80% of the sediment weight. Core YAM14-2A, located in the central part of the lake, has a stable grain size content with an average d90 of 54 $\mu m \pm 9$ μm. In core YAM14-1A, sedimentation is interrupted at a depth of 47.7 cm, by a 3-cm-thick coarser grained-layer showing cross-lamination interpreted as an instantaneous sedimentary event deposit (Figure 2). The background sedimentation consists of a high percentage of amorphous material (60–70%; Figure 3), which comprises a mixture of biogenic silica (diatoms) and allophane derived from weathering of volcanic tephra. The crystallized fraction is composed of total clays (24.3–36.5%), K-feldspar (37–52%; Figure 4), plagioclase (13–19%; Figure 4), and cristobalite (4–9%), which comprised the terrigenous fraction of the sediment. The correlation matrix shows a positive correlation ($r \geq 0.7$) between plagioclase, total clays, K-feldspar, and cristobalite. The clay fraction consists of illite and chlorite. A low proportion (<5%) of quartz, magnetite, calcite, and dolomite is also identified. The C/N ratio indicates that most of the OM present in the center of the Yamanaka basin is related to

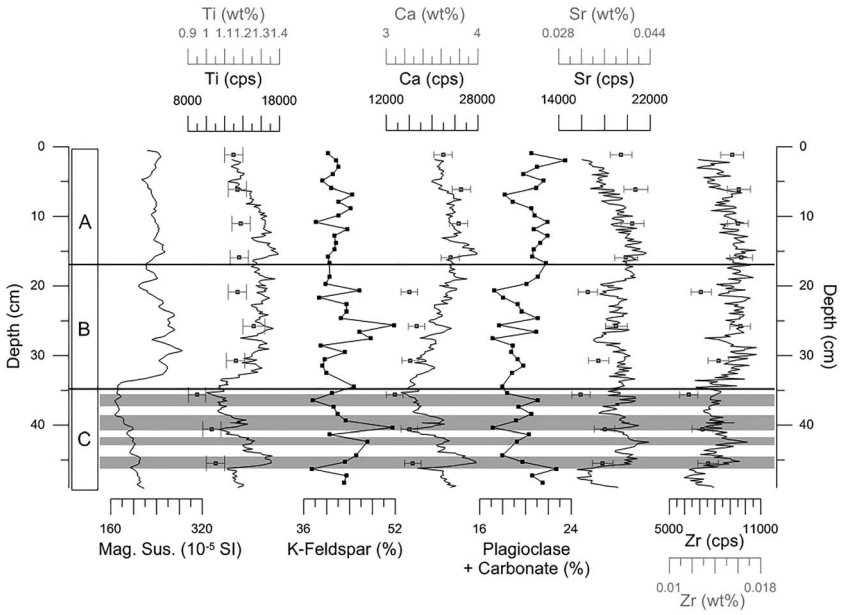

Figure 4. Depth profiles of the elements selected for study measured on YAM14-2A. (left to right) Magnetic Susceptibility Ti, percentage of K-feldpar, Ca (cps), Ca (wt%), percentage of plagioclases and carbonates, Sr (cps), Sr (wt%), Zr (cps), and Zr (wt%). Instrumental errors are represented by error bars on Ca (wt%), Sr (wt%), and Zr (wt%) depth profiles. Sedimentary boundaries (A–C) defined based on the magnetic susceptibility are shown as well. The peaks mentioned in the main text are highlighted in gray. We assume that these peaks are related to detrital pulses.

lake productivity (Figure 5). OM content calculated by loss on ignition (550 °C) shows a good correlation with TOC (r = 0.71) and TN (r = 0.80). By removing the TOC outlier value (at 8.5-cm depth), the correlation improves (r = 0.87).

4.2. Core Stratigraphy

The core stratigraphy is subdivided into four units on the basis of chemostratigraphy and magnetic susceptibility. Starting at the bottom of each core, Unit D is a layer of black scoria inferred to represent primary airfall tephra from the CE 1707 Hōei eruption. Units C, B, and A are described in more detailed in the following.

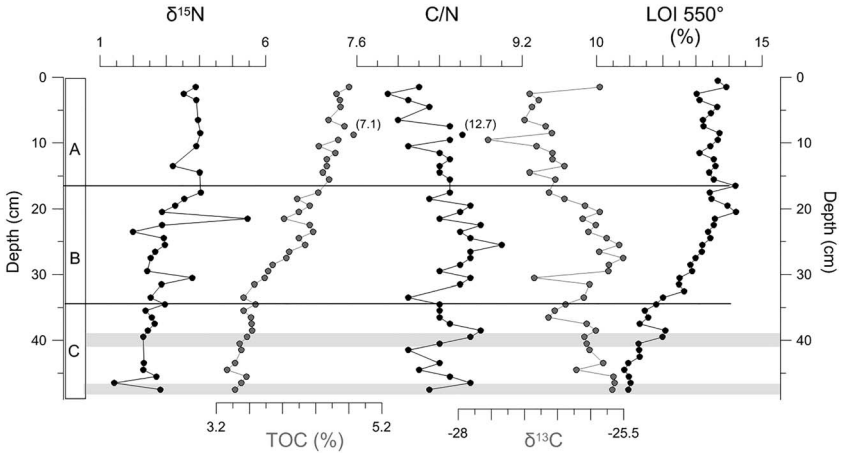

Figure 5. Depth profiles of the elements selected for study measured on YAM14-2A. (left to right) δ^{15}N, TOC (%), C/N, δ^{13}C, LOI for 550 °C (% OM). Sedimentary boundaries (A–C) defined based on the magnetic susceptibility are also represented. In Unit C, peaks of C/N associated or not with peak in % OM calculated from LOI at 550 °C coincide with peak of Si/Zr and are highlighted in gray. These peaks are interpreted as increase of in situ lake productivity. LOI = loss on ignition.

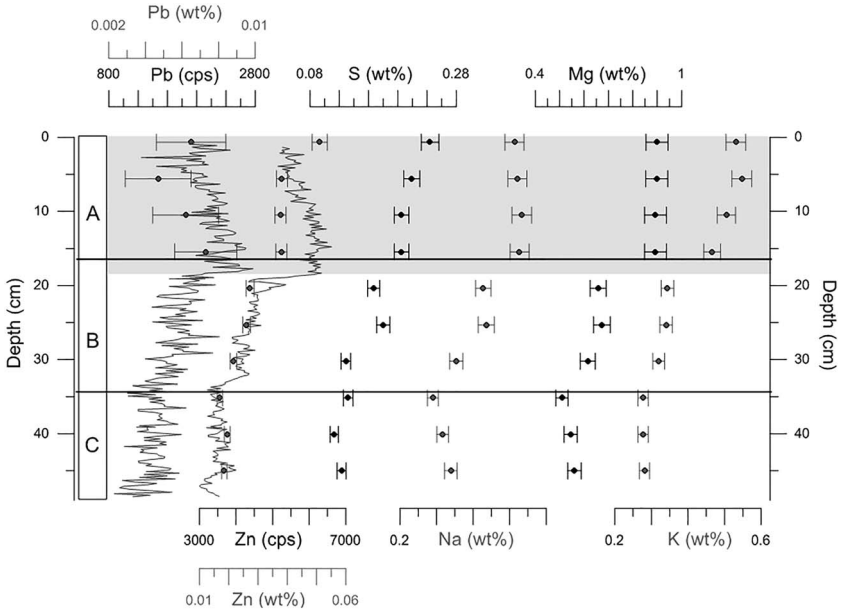

Figure 6. Depth profiles of the elements selected for study measured on YAM14-2A. (left to right) Pb (cps), Pb (wt%), Zn (cps), Zn (wt%), Na (wt%), Mg (wt%), K (wt%), and S (wt%). Errors bar indicated in the graph correspond to instrumental errors. Sedimentary boundaries (A–C) defined based on the magnetic susceptibility are shown as well. The recent increase of anthropogenic pollution is highlighted in gray.

4.2.1. Unit C

Unit C is characterized by a decreasing trend of magnetic susceptibility (Figure 4). The $\delta^{15}N$ values are relatively low (2.4 ± 0.4‰). Through Unit C, the Br/Ti ratio, OM, and TOC content tend to increase (Figure 3).

In this unit, Al, Si, and Ca are strongly correlated as well as Ca and Ti. Cu is associated with Zn, Sr, and Zr (supporting information S1). The base of Unit C presents low values of Ca, Sr, and Zr (Figure 4). Positive peaks of Ti, Ca, Sr, and Zr are observed at 44.6- to 45.6-cm, 42- to 43.2-cm, and 38.6- to 39.6-cm depths. Additionally, Ti and Sr show positive peaks at 36.0- to 37.2-cm depth (Figure 4). Within this sedimentary unit, Ca content shows a general decreasing trend until the upper boundary of the unit. Similarly to Ca, Si/Zr tends to decrease within the unit; three peaks of Si/Zr are identified at 46.8- to 49.2-cm depth, at 45- to 46.2-cm depth, and from 39.6 cm to the beginning of Unit B (33.2 cm; Figure 4). The first peak of Si/Zr is associated with a peak of TOC (Figure 5) and high Br/Ti content (Figure 4). The thicker one is correlated with a peak of OM content (Figure 5) and highest Br/Ti values (Figure 3). In the unit, Pb, Zn, Na (wt%), Mg (wt%), K (wt%), and S (wt%) are very stable (Figure 6).

4.2.2. Unit B

Unit B is defined by higher and stable magnetic susceptibility (Figure 4). Up to the upper boundary of Unit B, the $\delta^{13}C$ values tend to decrease; $\delta^{15}N$ values tend to increase upward from 2.5‰ to 4.0‰ with two positive peaks at 30.5- and 21.5-cm depths. Br/Ti tends to be constant (Figure 3). TOC and OM content increase through the unit. OM content reaches 14.2% at the upper boundary. In Unit B, there are two distinct associations of geochemical elements: (i) Ca, Si, and Al and (ii) Ca, Al, and Ti (supporting information). A global slight increase of Ca with several small peaks is observed. Ti, Sr, and Zr contents are mostly characterized by stable values with two low levels (Figure 4). From 34.4-cm depth up to the upper boundary of Unit B (19.8 cm), the profiles of Na (wt%), Mg (wt%), K (wt%), and S (wt%) present a global increase whereas Pb and Zn profiles tend to slightly increase up to 19.8-cm depth (Figure 6). The Si/Ti ratio (Figure 3) indicates a long-term increase trend, starting at 30-cm depth and continuing up to the top of the core (Unit A).

4.2.3. Unit A

Unit A presents stable magnetic susceptibility values (Figure 4) and OM content (from 13% to 14.2%—Figure 5). The high OM content in the upper part of the sedimentary infill is supported by smear slides, which show an enrichment of OM particles. The $\delta^{15}N$ values are generally stable and on average higher than in the previous units (3.9 ± 0.2‰). Like in Unit B, Br/Ti tends to be constant (Figure 3). In

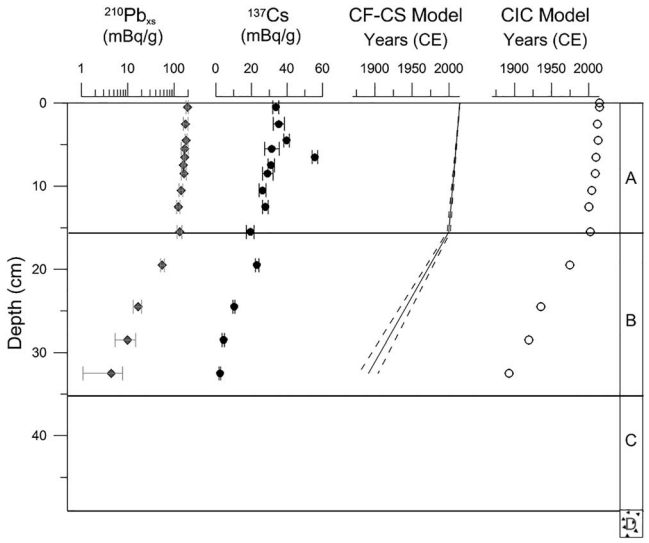

Figure 7. Age-depth model of YAM14-2A. From left to right, $^{210}Pb_{xs}$ depth profile, ^{137}Cs depth profile, CF/CS model and CIC model.

Unit A, a good correlation between Fe, Ti, Ca, Cu, Sr, and Zr is observed (supporting information S1). Unit A is characterized by a global decrease pattern for Ca as well as Sr and Zr (Figure 4). However, for Sr and Zr, the XRF results indicate that Sr (wt%) and Zr (wt%) content have highest values in Unit A (Figure 4) and remain stable suggesting that the top of the core is affected by a dilution effect related to OM content. We observe a decreasing trend of Ti (Figure 4). Pb, Zn, Na (wt%), Mg (wt%), and K (wt%) have the highest values. Pb slightly decreases upward with an exception for the upper 5 cm. Zn shows a decrease in the upper part of Unit A. However, similar to Sr and Zr, the decrease of Zn is not supported by XRF measurements, which show a stable behavior followed by an increase in the upper 5 cm. Na (wt%) and Mg (wt%) are stable, whereas K (wt%) and S (wt%) continue to increase (Figure 6).

4.3. Age-Depth Model

The chronology of the sedimentary infill of Lake Yamanaka is based on (i) ^{210}Pb dating and (ii) the presence of the Hōei scoria identified at the bottom of the cores.

In core YAM14-2A, the $^{210}Pb_{xs}$ profile shows two distinct trends with depth (Figure 7). First, its activity decreases slightly from 192 mBq/g at the surface down to 131 mBq/g at a depth of 15–16 cm, which indicates a rapid sediment accumulation rate. Second, the profile presents a rapid decrease of $^{210}Pb_{xs}$ activities to negligible values (<4 mBq/g) at a depth of 32–33 cm implying a lower sedimentation rate. The two distinct trends correspond to the boundary between the sedimentary Units A and B. The CF/CS (Oldfield & Appleby, 1984) was applied for the two distinct units (A and B) resulting in the following apparent sedimentation rate: 1.04 ± 0.14 cm/year for Unit A and 0.16 ± 0.01 cm/year for Unit B. ^{137}Cs, a byproduct of nuclear weapons fallout and nuclear accidents, is present in the atmosphere since 1950. Its high activities in the uppermost layers is associated with the 2011 Fukushima nuclear disaster. ^{137}Cs measurement reveals a peak of 56 mBq/g at 6.5-cm depth. The CF/CS model gives an age of CE 2009–2010 for the peak of ^{137}Cs and the constant initial concentration model dates the peak of ^{137}Cs at CE 2010. The shape of the ^{137}Cs peak suggests either bioturbation or a vertical migration of ^{137}Cs took place. No significant ^{210}Pb and ^{137}Cs concentrations were measured for Unit C. The sedimentation rate of Unit C (~0.09 cm/year) was estimated based on the occurrence of Hōei tephra at the bottom of the core and the inferred age of the upper boundary of Unit C. In the absence of ^{210}Pb and ^{137}Cs, we made the hypothesis that the sedimentation rate in Unit C in constant. Unit D corresponds to a near instantaneous event deposit, the CE 1707 Hōei eruption.

Based on the sedimentation rate obtained for Units A and B, the age of each sedimentary unit was defined. Unit C began after the Hōei eruption in CE 1707 and ended around CE 1885 ± 14. Unit B started around CE 1885 ± 14 and finished around CE 2000 ± 2. Unit A was deposited over a period of ~14 years, from circa CE 2000 ± 2 to CE 2014, the year of the coring campaign.

5. Interpretation and Discussion

5.1. The Impact of Scoria Fallout on the Lacustrine Sedimentation

The sedimentation rate prior the Hōei eruption can be estimated based on a drilling borehole taken 300 m far from YAM14-2A (see Figure 1 for the location). The ^{14}C dating done on plant remains indicates a sedimentation rate around ~0.16 ± 0.1 cm/year for the last ~1,400 years (Koshimizu et al., 2007). As the sedimentation accumulation rate is lower at the emplacement of the drilling borehole, we estimate that this sedimentation rate corresponds to a minimum (see Figure S1). Our results demonstrate that following the Hōei eruption, the posteruptive sedimentation rate was reduced by a factor of 2 (~0.09 cm/year). This is in contrast with previous studies (e.g., Hayes et al., 2002; Major et al., 1996; Ollier & Brown, 1971; Pierson et al., 1992), documenting the highest sedimentation following an eruption. High-sedimentation rates are mainly linked to remobilization of ash-fallout deposits by fluvial or mass-flow processes. In the sedimentary sequence of Lake Yamanaka, no fine-grained tephra fallout deposits have been identified, due to its proximal

location to Mount Fuji. After the Hōei eruption, a thick scoria layer (thickness up to 64 cm; Miyaji et al., 2011) covered Lake Yamanaka and its catchment (Figure 1a). Sr and Zr measurements (Figure 4), proxies for the presence of a terrigenous signal, indicate very low terrigenous input in the aftermath of the Hōei eruption. During the first ~170 years after the Hōei eruption (Unit C), the sedimentation was detrital driven (cf. detrital pulses identified in Ti, Ca, Sr, and Zr peaks in Figure 4). These detrital pulses are sometimes accompanied by peak measurements of amorphous materials, K-feldspar, and/or plagioclase (Figures 3 and 4). The observed low sedimentation rate and sedimentary pulses over the first 170 years following the Hōei eruption can be explained. Deposition of the up to 64-cm-thick Hōei scoria increased surface permeability, in addition to sealing off erodible and loose volcanic soils from erosion and transport processes. The erosion and transport of scoria deposits requires high energy events, such as typhoons or earthquake shaking. During intense episodic typhoons, increased rainfall water percolated through the thick Hōei scoria layer, inducing saturation and decreasing the resistance of the scoria deposits against erosion by surface runoff. In the catchment, surface runoff initiated the erosion and transport of the Hōei scoria and the sediment below, toward Lake Yamanaka. The latter explains the presence of a series of four sedimentary pulses, rich in terrigenous material, recorded in the central part of the lake (Figure 4). Other mechanisms, such as earthquake shaking and mass movement might also trigger episodic increases in sediment transport toward Lake Yamanaka.

Since CE 1885 ± 14 (base of Unit B), the detrital supplies toward the lake became more important, as indicated in our cores by an increase in the sedimentation rate and magnetic susceptibility and Ca content (Figure 4) associated with the presence of plagioclase and carbonate. The terrigenous content became more stable, indicating that moderate rainfalls had sufficient energy to erode and transport surface sediment from the watershed toward Lake Yamanaka. The erosion and transport of the Hōei scoria deposits (decreasing its thickness) during typhoons, the development of a new soil on top of the Hōei scoria deposits, and agricultural practices influenced sedimentation within Lake Yamanaka. Lake Yamanaka's sedimentary system needed at least ~170 years to begin to recover from the deposition of the thick Hōei scoria in its catchment and to restore the sedimentation rate to before CE 1707 levels.

5.2. Sedimentation Recovery and Human Impact

From CE 1885 ± 14 to CE 2000 ± 2, the average sedimentation rate is similar to the one before the Hōei eruption. It is difficult to assess to what extent sedimentation recovery was accelerated by human activities and/or natural processes. Indeed, during this period, Lake Yamanaka's catchment was the subject of changes in land occupation (i.e., urbanization, deforestation, and agriculture).

Especially during the last century, urbanization modified the catchment of Lake Yamanaka and many roads and houses as well as larger infrastructure were built. Since 1936–1938, a military base occupied 12% of the catchment. Before the 1960s, the base was used by U.S. army mainly for military drills. In the 1980s, a 3 km tunnel was built in the southwest of Lake Yamanaka. The direct consequence of construction works are the large quantities of sediment available in the catchment due to excavations. Moreover, road surfaces limit water infiltration and increase erosion and transport of fine-grained materials (e.g., Dunne, 1979; Fahey & Coker, 1989; Reid & Dunne, 1984). High sedimentation rates are observed in the years directly following road constructions and decrease over time (Fredriksen, 1970; Megahan & Kidd, 1972).

From 1900 to 1950, timber harvest was a standard forestry practice in Japan (Paletto et al., 2008). Deforestation of coniferous and broadleaf forest took place to provide wood supplies for building and heating. It is well known that deforestation leads to an increase of sedimentation rate in a catchment (Grant & Wolff, 1991). The recovery rate is variable and depends on the nature of the disturbance. Surficial mass movements, related to root decay, can occur decades after harvesting (Grant & Wolff, 1991). Since the 1970s–1980s, people began to use fossil fuels instead of wood for heating in Japan, initiating the recovery of forest (S. Yamamoto, personal communication, 2017 and Figure 8).

Aerial photographs taken in 1948 (Figures 8a and 8g) show numerous small cultivated parcels, delimited by strips of vegetation planted perpendicular to the slopes. The use of vegetated strips reduces surface runoff and soil erosion (e.g., Barfield et al., 1975; Dillaha et al., 1989), slowing down terrestrial inputs of water, trapping sediment, and filtering nutrients (Yuan et al., 2009). The vegetated strips present around the Lake Yamanaka, as shown on aerial photographs (Figures 8a, 8c, and 8g), trap the sediment in the catchment

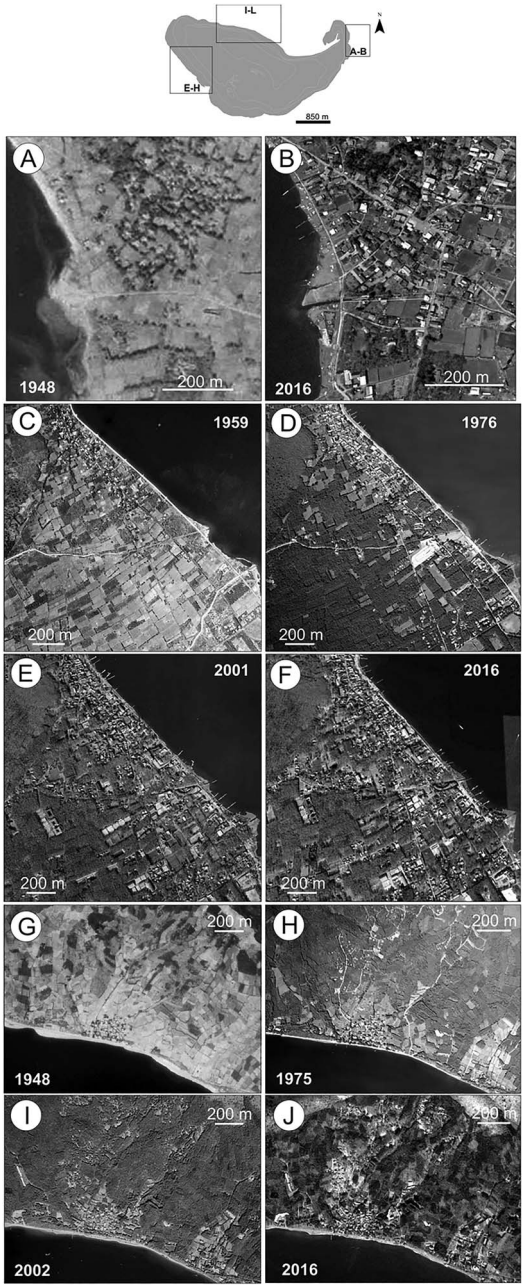

Figure 8. Landscape evolution and land change occupation. (a) Aerial photograph of the eastern part of Lake Yamanaka in 1948 (GSI, 2017). (b) Landsat photograph of the eastern part of Lake Yamanaka in 2016 (Google Earth, April 24, 2016). In the eastern part of Lake Yamanaka, the cultivated parcels present in 1948 were progressively replaced by houses and buildings. In some places, cultivated parcels were merged into bigger parcels. Nowadays, vegetated strips are mostly absent. (c) Aerial photograph of the southwestern part of Lake Yamanaka in 1959 (GSI, 2017). (d) Aerial photograph of the southwestern part of Lake Yamanaka in 1976 (GSI, 2017). (e) Aerial photograph of the southwestern part of Lake Yamanaka in 2001 (GSI, 2017). (f) Landsat photograph of the southwestern part of Lake Yamanaka in 2016 (Google Earth, April 24, 2016). From 1959 to 1976, cultivated parcels almost disappeared and were replaced by forest. Occasionally, cultivated parcels were still present. From 1976 to 2016, urbanization grew in the southwestern of the lake. Houses, buildings, and roads were constructed leading to a decrease of the forest area and cultivated parcels. Landscape Evolution and Land change occupation. (g) Aerial photograph of the northern part of Lake Yamanaka in 1948 (GSI, 2017). (h) Aerial photograph of the northern part of Lake Yamanaka in 1975 (GSI, 2017). (i) Aerial photograph of the northern part of Lake Yamanaka in 2002 (GSI, 2017). (j) Landsat photograph of the northern part of Lake Yamanaka in 2016 (Google Earth, April 24, 2016). In 1948, the north of the lake was entirely cultivated and a small village occupied its border. From 1948 to 1975, cultivated lands were progressively abandoned and replaced by forest. From 1975 to 2016, the north border of Lake Yamanaka has been urbanized.

and reduce the influence of other human impacts (construction of buildings and roads, and forest harvesting) on the sedimentation rate. During the second half of the twentieth century, small cultivated parcels progressively disappeared and were replaced by larger cultivated parcels, houses, or forest (Figures 8a, 8d–8f, and 8h–8j). Moreover, the numerous roads parallel to the slope help increase the sediment input from the catchment toward the lake. During the last decade, the decrease of agriculture and vegetated strips combined with the increase of urbanization around Lake Yamanaka lead to an increase in the sedimentation rate by a factor ~6. From a sedimentological point of view, the decline of agriculture and the increase of human activities have a larger impact on the sedimentation rate of Lake Yamanaka than the Hōei eruption.

5.3. Lake Productivity and Volcanic Eruption

The Hōei eruption did not only affect the sedimentation rate of Lake Yamanaka but also influenced the lake productivity. Following the Hōei eruption, the presence of peaks of Si/Zr, TOC, and the high content of Br/Ti in our measurements indicate the occurrence of algal blooms (Figure 3). An increase in diatom concentrations following the deposition of volcanic ash layers has been documented in several paleoenvironmental studies (e.g., Smith & White, 1985; Telford et al., 2004). Deposition of volcanic ash into lacustrine environments leads to the dissolution of adsorbed metal salts, acid, and aerosols, increasing the concentration of key nutrients (Frogner et al., 2001). Experiments conducted by Jones and Gislason (2008) on several ash layers show that in contact with water, the fluxes of important macronutrients (such as Si, P, and Fe) and of key micronutrients (Mn, Co, Ni, Cu, and Zn) increases. Bioincubation experiments have shown that diatoms use nutrients from volcanic ash (Duggen et al., 2007). Considering the deposition of scoria fallout, similar process may play a role. Nutrient fluxes might be less important than in the case of a fine ash layer, as smaller particles are better scavengers of volatiles due to their higher surface area to mass ratio (Oskarsson, 1980). The Hōei eruption induced volcanogenic fertilization of Lake Yamanaka resulting in an increase in diatom concentration in the sediments (evidenced by Si/Zr ratios) recorded for over a period of $\geq$35 years (Figure 3).

Around CE 1830, a second increase of diatoms (Si/Zr) and lake productivity (high Br/Ti content and peak of OM) is observed. The presence of a peak in K-feldspar reaching 52% in our measurements (Figure 4) is evidence of a strong catchment disturbance.

5.4. Fertilizers, Lake Productivity, and Eutrophication

Since CE 1880, in-lake productivity (OM content, TOC) increased as well as diatom content (Si/Zr; Figures 3 and 5). Moreover, euglenophycean and chlorophycean algae are present in the sediment (Yamagishi et al., 1982). The increase of OM produced in Lake Yamanaka can be linked to an increase of nutrient supplies, enhanced by catchment erosion and fertilizers used for the cultivation of rice and mulberries. The δ^{15}N signature (Figure 5) recorded in the sediment suggests the use of synthetic fertilizers, characterized by values between −4‰ and +4‰ (Kendall, 1998). The increase of Na, Mg, and K contents is related to the presence of chemical fertilizers (e.g., fused magnesium phosphate) used in Japan during the 1970s (Koshino, 1990).

Despite the decline of agriculture since the second half of the century, the Na, Mg, and K contents remained relatively high until the present day (Figure 6). For decades, contaminated sediments were trapped in the vegetated strips. With their decrease and the increase of excavations in the 2000s, polluted sediments were remobilized and transported to Lake Yamanaka, explaining the time delay between the period of fertilizer use in the catchment and their recording in Lake Yamanaka. Additionally, fertilizers might have contaminated ground water, which is the main water source of Lake Yamanaka.

The higher concentration of OM since CE 2000 $\pm$ 2 and the significant increase of P over the last 5 years suggest eutrophication of Lake Yamanaka. Lake Yamanaka was classified as a mesotrophic lake by Aizaki et al. (1981). Hirabayashi et al. (2004) suggest that the trophic status of the lake should be reconsidered based on an increase of the density of *Propsilocerus akamusi* larvae and their positive correlation with OM. However, no notable change of chlorophyll *a* content is observed for the last 20 years (Yamanashi Prefecture, 2015). The high in situ lake productivity contributes to the increased sedimentation rate (i.e., increase of the organic compound) recorded in the last decade.

5.5. Atmospheric Pollution

The poor correlation between Pb, Ti, Br, and OM suggests that Pb enrichment is not governed by OM concentration and is not related to the catchment area. Therefore, Pb enrichment is directly linked to atmospheric pollution from coal burning and gasoline pollution. The atmospheric pollution (Pb and Zn) started to increase from around ~CE 1885 ± 14 (base of Unit B, Figure 6). This observation corresponds to the beginning of Japanese industrialization that started around the 1870s (Hayami et al., 2004). From the beginning of the 1980s, significant enrichment of Pb, Zn, and S is noticed in the sediment of Lake Yamanaka. An air monitoring station located at the summit of Mount Fuji indicates that the troposphere is affected by significant amounts of polluted air from China and from Japan itself (Suzuki et al., 2008). The recent industrialization of China and its growth is probably responsible for the recent increase of atmospheric pollution recorded in Lake Yamanaka.

6. Conclusions

This study highlights the impact of scoria fallout on a lacustrine system. The Hōei scoria fallout (CE 1707) had two major impacts on Lake Yamanaka: (i) reduction of the sedimentation rate and (ii) a peak of lake productivity. The sedimentation rate after a Plinian eruption is relatively low due to the deposition of a thick scoria layer trapping the underlying sediments. This contrast with previous studies where an increase of sedimentation rate is usually observed following ash fallout deposits. This study suggests that the sedimentation rate is affected by the grainsize of the volcanic ejecta. Coarse-grained tephra such as scoria are difficult to erode by rain splash and surface runoffs. The erosion of the catchment occurred during intense typhoons when porous scoria layers are saturated by heavy rains. The heavy rains trigger surface runoffs which drained the sediments from the catchment toward the lake. Lake Yamanaka needed more than ~170 years to begin to recover toward similar sedimentation rate (~0.16 cm/year) that existed before the Hōei eruption. The recovery might have been accelerated by land use changes. During the last decade, the sedimentation rate increased drastically due to the decline of agriculture and planting of vegetated strips, urbanization of the catchment and the increase of in situ lake productivity. Anthropogenic modifications of the catchment have greater impacts on the sedimentation rate than a major volcanic eruption. Moreover, agriculture and industrialization have severely contaminated Lake Yamanaka.

Acknowledgments
This research was undertaken as part of the QuakeRecNankai project, funded by the Belgian Science Policy Office (BELSPO BRAIN-be BR/121/A2). Additional sponsorship were provided by Camille Hela foundation and by the Marie-Louise Léonard grant. The members of the QuakeRecNankai team (Ed Garrett, Atsunori Nakamura, Stephen Obrochta, Masanobu Shishikura, Yosuke Miyairi, Helmut Brückner, Eisuke Ono, Svenja Riedesel, Koen De Rycker, Yoshiki Sato, and Jan Walstra) are acknowledged for their help and their technical support during the fieldwork surveys. We thank the Mount Fuji Research Institute for their collaboration and their logistical support. We are thankful to Ellynn Bertemes (University of Liège) and to Thomas Goovaerts (Geological survey of Belgium) for their lab work. We are grateful to the EDYTEM laboratory and to Anne-Lise Develle for the use of the Avaatech scanner. We are thankful to the French Nouvelle Aquitaine Research Council (E3A Project) for the funding of the low-background gamma detector. We are thankful to Dr. Vern Manville and one anonymous reviewer for constructive feedback that significantly improved the manuscript. Laura Lamair is currently funded by BELSPO. All the data used are listed in the references or archived in ORBI repository (http://hdl.handle.net/2268/229301).

References

Adhikari, D.P., Koshimizu, S., & Uchiyama, T. (2005). Variation in particle size distribution in the core sediment of Lake Yamanaka, northeastern foot of Mt. Fuji and its paleoenvironmental significance. *Proceeding of the 15th symposium on Geo-environments and Geo-Technics,* 191–196.

Agnihotri, R., Altabet, M. A., Herbert, T. D., & Tierney, J. E. (2008). Subdecadally resolved paleoceanography of the Peru margin during the last two millennia. *Geochemistry, Geophysics, Geosystems*, *9*, Q05013. https://doi.org/10.1029/2007GC001744

Aizaki, M., Otsuki, A., Fukushima, T., Kawai, T., Hosomi, M., & Muraoka, K. (1981). Application of modified Carlson's trophic state index to Japanese lakes and its relationships to other parameters related to trophic state (in Japanese with English summary). *Research Report from the National Institute for Environmental Studies Japan*, *23*, 13–31.

Barfield, B. J., Kao, D. T. Y., & Tollner, E. W. (1975). *Analysis of the sediment filtering action of grassed media*. Research Paper 90. Lexington: University of Kentucky, Water Research Institute.

Collins, B. D., & Dunne, T. (1986). Erosion of tephra from the 1980 eruption of Mount St. Helens. *Geological Society of America Bulletin*, *97*(7), 896–905. https://doi.org/10.1130/0016-7606(1986)97<896:EOTFTE>2.0.CO;2

Collins, B. D., Dunne, T., & Lehre, A. K. (1983). Erosion of tephra-covered hillslopes north of Mount St. Helens, Washington: May 1980-May 1981. *Zeitschrift für Geomorphologie Suppl. Bd*, *46*, 103–121.

Cuven, S., Francus, P., & Lamoureux, S. (2011). Mid to Late Holocene hydroclimatic and geochemical records from the varved sediments of East lake, Cape Bounty, Canadian High Arctic. *Quaternary Science Reviews*, *30*(19-20), 2651–2665. https://doi.org/10.1016/j.quascirev.2011.05.019

Dillaha, T. A., Reneau, R. B., Mostaghimi, S., & Lee, D. (1989). Vegetative filter strips for agricultural nonpoint source pollution control. *Transactions of the ASAE*, *32*(2), 0513–0519. https://doi.org/10.13031/2013.31033

Duggen, S., Croot, P., Schacht, U., & Hoffmann, L. (2007). Subduction zone volcanic ash can fertilize the surface ocean and stimulate phytoplankton growth: Evidence from biogeochemical experiments and satellite data. *Geophysical Research Letters*, *34*, L01612. https://doi.org/10.1029/2006GL027522

Dunne, T. (1979). Sediment yield and land use in tropical catchments. *Journal of Hydrology*, *42*(3-4), 281–300. https://doi.org/10.1016/0022-1694(79)90052-0

Fahey, B. D., & Coker, R. J. (1989). Forest road erosion in the granite terrain of southwest Nelson, New Zealand. *Journal of Hydrology (New Zealand)*, *28*, 123–141.

Folsom, M. M. (1986). Tephra on range and forest lands of eastern Washington: Local erosion and redeposition. In *Mount St Helens: Five years later* (pp. 116–119). Washington: Eastern Washington University Press.

Fredriksen, R. L. (1970). Erosion and sedimentation following road construction and timber harvest on unstable soils in three small western Oregon watersheds. USDA Forest Service, Pacific Northwest Forest and Range Experiment Station Research Paper PNW- 104: Portland, Oregon.

Frogner, P., Gislason, S. R., & Oskarsson, N. (2001). Fertilizing potential of volcanic ash in ocean surface water. *Geology*, *29*(6), 487–490. https://doi.org/10.1130/0091-7613(2001)029<0487:FPOVAI>2.0.CO;2

Google Earth V. 7.1.8.3036. (April 24, 2016). Lake Yamanaka, Honshu Island. 35°24′57″N, 138°52′29″E, Eye alt 2000 m. Landsat, Copernicus. Retrieved from http://www.earth.google.com [August 16, 2017].

Grant, G. E., & Wolff, A. L. (1991). Long-term patterns of sediment transport after timber harvest, Western Cascade Mountain, Oregon, USA. In *Sediment and stream water quality in a changing environment: Trends and explanation* (pp. 31–40). Wallingford, Oxfordshire, UK: IAHS publication 203.

GSI (2017). Geospatial information authority of Japan. Global map. Retrieved from http://maps.gsi.go.jp, consulted on August 18, 2017.

Hayami, A., Saito, O., & Tobey, R. (Eds.) (2004). *Emergence of economic society in Japan* (pp. 1600–1859). Oxford: Oxford University Press.

Hayes, S. K., Montgomery, D. R., & Newhall, C. (2002). Fluvial sediment transport and deposition following the 1991 eruption of Mount Pinatubo. *Geomorphology*, *45*(3–4), 211–224.

Heiri, O., Lotter, A. F., & Lemcke, G. (2001). Loss on ignition as a method for estimating organic and carbonate content in sediments: Reproducibility and comparability of results. *Journal of Paleolimnology*, *25*(1), 101–110. https://doi.org/10.1023/A:1008119611481

Hirabayashi, K., Yoshizawa, K., Yoshida, N., & Kazama, F. (2004). Progress of eutrophication and change of chironomid fauna in Lake Yamanakako, Japan. *Limnology*, *5*(1), 47–53. https://doi.org/10.1007/s10201-003-0113-2

Jones, M. T., & Gislason, S. R. (2008). Rapid releases of metal salts and nutrients following the deposition of volcanic ash into aqueous environments. *Geochimica et Cosmochimica Acta*, *72*(15), 3661–3680. https://doi.org/10.1016/j.gca.2008.05.030

Kendall, C. (1998). Tracing nitrogen sources and cycles in catchments. In C. Kendall & J. J. McDonnell (Eds.), *Isotope tracers in catchment hydrology* (pp. 519–576). Amsterdam: Elsevier.

Koshimizu, S., & Tomura, K. (2000). Geochemical behavior of trace vanadium in the spring, groundwater, and lake water at the foot of Mt. Fuji, central Japan. In K. Sato & Y. Iwasa (Eds.), *Groundwater updates* (pp. 171–176). Tokyo, Japan: Springer-Verlag.

Koshimizu, S., Uchiyama, T., & Yamamoto, G. (2007). Volcanic history of Mt. Fuji recorded in borehole cores from Fuji Five Lakes surrounding Mt. Fuji. Fuji. In S. Aramaki, T. Fujii, S. Nakada, & N. Miyaji (Eds.), *Fuji Volcano* (in Japanese with English abstract) (pp. 365–374). Yamanashi: Yamanashi Institute of Environmental Sciences.

Koshino, M. (1990). *The use of organic and chemical fertilizers in Japan. Extension bulletin 312*. Taipei: Food and Fertilizer Technology center.

Kylander, M., Ampel, L., Wohlfarth, B., & Veres, D. (2011). High-resolution X-ray fluorescence core scanning analysis of Les Echets (France) sedimentary sequence: new insights from chemical proxies. *Journal of Quaternary Science*, *26*(1), 109–117. https://doi.org/10.1002/jqs.1438

Lamair, L., Hubert-Ferrari, A., Yamamoto, S., Fujiwara, O., Yokoyama, Y., Garrett, E., et al. (2019). Use of high-resolution seismic reflection data for paleogeographical reconstruction of shallow Lake Yamanaka (Fuji Five Lakes, Japan). *Palaeogeography Palaeoclimatology Palaeoecology*, *514*, 233–250. https://doi.org/10.1016/j.palaeo.2018.09.028

Major, J. J., Bertin, D., Pierson, T. C., Amigo, A., Iroumé, A., Ulloa, H., & Castro, J. (2016). Extraordinary sediment delivery and rapid geomorphic response following the 2008–2009 eruption of Chaitén Volcano, Chile. *Water Resources Research*, *52*, 5075–5094. https://doi.org/10.1002/2015WR018250

Major, J. J., Janda, R. J., & Daag, A. S. (1996). Watershed disturbance and lahars on the east side of Mount Pinatubo during the mid-June 1991 eruptions. In C. G. Newhall & R. S. Punongbayan (Eds.), *Fire and mud, eruptions and lahars of Mount Pinatubo, Philippines* (pp. 895–920). Quezon City, and University of Washington Press, Seattle: PHIVOLCS Press.

Manville, V., Nemeth, K., & Kano, K. (2009). Source to sink: A review of three decades of progress in the understanding of volcaniclastic processes, deposits, and hazards. *Sedimentary Geology*, *220*(3-4), 136–161. https://doi.org/10.1016/j.sedgeo.2009.04.022

Manville, V., Segschneider, B., Newton, E. H., White, J. L. D., Houghton, B. F., & Wilson, C. J. N. (2009). Environmental impact of the 1.8 ka Taupo eruption: Landscape responses to a large-scale explosive rhyolitic eruption. *Sedimentary Geology*, *220*(3-4), 318–336. https://doi.org/10.1016/j.sedgeo.2009.04.017

Manville, V., & Wilson, C. J. N. (2004). The 26.5 ka Oruanui eruption, New Zealand: A review of the roles of volcanism and climate in the post-eruptive sedimentary response. *New Zealand Journal of Geology and Geophysics*, *47*(3), 525–547. https://doi.org/10.1080/00288306.2004.9515074

Megahan, W. F., & Kidd, W. J. (1972). Effect of logging roads on sediment production rates in the Idaho batholith. USDA Forest Service, Intermountain Forest and Range Experiment Station Research Paper INT-123: Ogden, Utah.

Meyers, P. A. (1994). Preservation of elemental and isotopic source identification of sedimentary organic matter. *Chemical Geology*, *114*(3-4), 289–302. https://doi.org/10.1016/0009-2541(94)90059-0

Miyaji, N., Kan'no, A., Kanamaru, T., & Mannen, K. (2011). High-resolution reconstruction of the Hoei eruption (AD 1707) of Fuji volcano, Japan. *Journal of Volcanology and Geothermal Research*, *207*(3-4), 113–129. https://doi.org/10.1016/j.jvolgeores.2011.06.013

Moore, D. M., & Reynolds, R. C. (1989). *X-ray diffraction and the identification and analysis of clay minerals* (332 pp.). Oxford: Oxford University Press.

Oldfield, F., & Appleby, P. G. (1984). Empirical testing of Pb-210-dating models for lake-sediments. In E. Y. Haworth & J. G. Lund (Eds.), *Lake sediments and environmental history* (pp. 93–124). Leicester: Leicester University Press.

Ollier, C. D., & Brown, M. J. F. (1971). Erosion of a young volcano in New Guinea. *Zeitschrift fuer Geomorphologie*, *15*(1), 12–28.

Oskarsson, N. (1980). The interaction between volcanic gases and tephra: Fluorine adhering to tephra of the 1970 Hekla eruption. *Journal of Volcanology and Geothermal Research*, *8*(2-4), 251–266. https://doi.org/10.1016/0377-0273(80)90107-9

Ozaki, M., Makimoto, H., Sugiyama, Y., Mimura, K., Sakai, A., Kubo, K., et al. (2002). *Geological map of Japan 1: 200 000, Kofu* (in Japanese with English abstract). Tsukuba, Japan: Geological Survey of Japan, AIST.

Paletto, A., Sereno, C., & Furuido, H. (2008). Historical evolution of forest management in Europe and in Japan. *Bulletin of the Tokyo university forests*, *119*, 25–44.

Pierson, T. C., Janda, R. J., Umbal, J. V., & Daag, A. S. (1992). Immediate and long-term hazards from lahars and excess sedimentation in rivers draining Mt. Pinatubo, Philippines. U.S. Geological Survey Water-Resources Investigations Report 92–4039 (35 pp.).

Pierson, T. C., & Major, J. J. (2014). Hydrogeomorphic effects of explosive volcanic eruptions on drainage basins. *Annual Review of Earth and Planetary Sciences*, *42*(1), 469–507. https://doi.org/10.1146/annurev-earth-060313-054913

Pierson, T. C., Major, J. J., Amigo, A., & Moreno, H. (2013). Acute sedimentation response to rainfall following the explosive phase of the 2008-2009 eruption of Chaitén volcano, Chile. *Bulletin of Volcanology*, *75*(5), 723. https://doi.org/10.1007/s00445-013-0723-4

Reid, L. M., & Dunne, T. (1984). Sediment production from road surfaces. *Water Resources Research*, *20*(11), 1753–1761. https://doi.org/10.1029/WR020i011p01753

Schmidt, S., & De Deckker, P. (2015). Present-day sedimentation rates on the southern and southeastern Australian continental margins. *Australian Journal of Earth Sciences*, *62*(2), 143–150. https://doi.org/10.1080/08120099.2015.1014846

Smith, M. A., & White, M. J. (1985). Observations on lakes near Mount St. Helens: phytoplankton. *Archiv für Hydrobiologie*, *104*, 345–362.

Suzuki, I., Hayashi, K., Igarashi, Y., Takahashi, H., Sawa, Y., Ogura, N., et al. (2008). Seasonal variation of water-soluble ion species in the atmospheric aerosols at the summit of Mt. Fuji. *Atmospheric Environment*, *42*(34), 8027–8035. https://doi.org/10.1016/j.atmosenv.2008.06.014

Telford, R. J., Barker, P., Metcalfe, S., & Newton, A. (2004). Lacustrine responses to tephra deposition: Examples from Mexico. *Quaternary Science Reviews*, *23*(23-24), 2337–2353. https://doi.org/10.1016/j.quascirev.2004.03.014

Tsuya, H. (1955). Geological and petrological studies of volcano, Fuji, V.: 5. On the 1707 eruption of Volcano Fuji. *Bulletin of the Earthquake Research Institute, University of Tokyo*, *33*, 341–383.

White, J. D. L., Houghton, B. F., Hodgson, K. A., & Wilson, C. J. N. (1997). Delayed sedimentary response to the CE 1886 eruption of Tarawera, New Zealand. *Geology*, *25*(5), 459–462. https://doi.org/10.1130/0091-7613(1997)025<0459:DSRTTA>2.3.CO;2

Yamagishi, T., Ooshima, K., & Watanabe, M. (1982). Plankton algae from Fuji Goko. *Memoirs of the National Museum of Nature and Science, Tokyo*, *15*, 91–97.

Yamanashi Prefecture (2015). *The water quality of the Fuji Five Lakes over 44 years (in Japanese)*. Kofu: Yamanashi Prefecture. Retrieved from http://www.pref.yamanashi.jp/taiki-sui/sokutei.html

Yuan, Y., Bingner, R. L., & Locke, M. A. (2009). A review of effectiveness of vegetative buffers on sediment trapping in agricultural areas. *Ecohydrology*, *2*(3), 321–336. https://doi.org/10.1002/eco.82